


RESEARCH ARTICLE

# Dynamics and control of a high-altitude balloon with slung load

L. Chen , Z. Song and J. Lin

School of Air Transportation, Shanghai University of Engineering Science, Shanghai, China

Corresponding author: L. Chen; Email: [cl@sues.edu.cn](mailto:cl@sues.edu.cn)

Received: 5 July 2023; Revised: 30 December 2023; Accepted: 25 June 2024

Keywords: high-altitude balloon; slung-load dynamics; altitude regulation; cable force

## Abstract

The high-altitude balloon proposed in this paper is a long-life balloon carrying a payload through a cable that flies at 20km altitude in near space. A dynamic model of the system, including the thermodynamics of the buoyancy body coupled with a hanging model of the pod, is developed using the Newton–Euler method. The buoyancy body consists of a helium balloon and a ballonnet. A differential pressure difference-based altitude adjustment is achieved by tracking the pressure difference at the target altitude. A dynamic simulation of the buoyancy body with a slung pod in autonomous vertical takeoff and altitude regulation processes is presented. The internal thermodynamic variations and pressure differential of the buoyancy body are given. The air mass exchange and blower flow control of the ballonnet are validated. The altitude holding error is analysed. The maximum pull force that the cable can withstand is calculated, and the maximum attitude angles of the pod during the ascending and descending processes are depicted. Simulation results provide basic knowledge for the structural design and payload installation of pods.

## Nomenclature

$a$	solar radiation absorption efficiency
$\mathbf{a}_p$	inertial acceleration of the pod expressed in the body coordinate system
$A_1$	solar radiation absorption area
$A_2$	heat transfer area between the balloon and the environment
$A_3$	heat transfer area between <i>internal air and helium</i>
$B = \rho V$	buoyancy of the balloon
$C_D$	aerodynamic drag coefficient of the pod
$C_{p,He}, C_{p,air}$	specific heat of helium and air
$C_X, C_Y, C_Z, C_l, C_m, C_n$	aerodynamic coefficients of the balloon
$\mathbf{F}_{pA}$	aerodynamic force on the pod
$\mathbf{F}_{pG}$	gravity of the pod
$\mathbf{F}_{pL}$	cable force on the pod
$\mathbf{F}_{pI}$	inertial force on the pod
$I$	<i>solar radiation absorption constant</i>
$I_x, I_y, I_z$	<i>inertial moments of the balloon</i>
$k$	volume ratio of the helium balloon to the ballonnet
$K_1$	heat transfer coefficient between the balloon and the environment
$K_2$	heat transfer coefficient between internal air and helium
$l$	cable length
$l_{ref}$	reference length of the balloon
$L_{He}$	net lift from the buoyancy body
$m$	total mass of the balloon
$m_p$	pod mass

$m_{Air}, m_{He}$	internal air mass and helium mass
$m_{stru}$	mass of the mechanical structure of the body
$m_{add}$	additional mass for the balloon
$M_{Air}$	molar mass of air
$o_s, x_s, y_s, z_s$	suspension point coordinate system
$o_b, x_b, y_b, z_b$	body coordinate system
$\mathbf{p} = [x_p, y_p, z_p]^T$	pod position in the body coordinate system
$P, P_{He}, P_{Air}$	pressure of the reference air, internal helium and internal air
$Q$	dynamic pressure
$R = 8.314 \text{ J/K/mol}$	universal gas constant
$R_{Air} = 286.7 \text{ J/kg/K}$	gas constant of air
$R_{He} = 2078.6 \text{ J/kg/K}$	gas constant of helium
$\mathbf{s} = [0, 0, d]^T$	suspension point position in the body coordinate system
$S$	reference area of the balloon
$S_p$	reference area of the pod
$T, T_{He}, T_{Air}$	temperature of the reference air, internal helium and internal air
$V_{He}, V_{Air}$	helium balloon volume and ballonet volume
$V = V_{Air} + V_{He}$	total volume of the balloon
$\mathbf{V}_o = [u \ v \ w]^T$	linear velocity of the balloon
$\mathbf{V}_p = [u_p \ v_p \ w_p]^T$	linear velocity of the pod
$\mathbf{V}_w = [u_w \ v_w \ w_w]^T$	wind velocity vector in the body coordinate system
$X_a, Y_a, Z_a, L_a, M_a, N_a$	aerodynamic force and moment components in the balloon
$\boldsymbol{\omega} = [p \ q \ r]^T$	angular velocity of the balloon
$\theta_L, \phi_L$	forward angle and lateral angle of inclination of the pod
$\phi, \theta, \psi$	Euler angles of the balloon
$\rho$	reference atmospheric density
$\rho_{Air}$	air density inside the ballonet
$\rho_{He}$	helium density inside the balloon
$\rho_{He0}$	helium density under a normal pressure
$\Delta P_{max}$	maximum pressure difference for the envelope to withstand
$\Delta$	differential pressure difference between current and target altitudes
$\delta$	pressure difference change threshold
$\delta P_{He}$	pressure difference between the inside and outside of the balloon
$\delta P_{Air}$	pressure difference between the inside and outside of the ballonet
$\delta T_{He}$	temperature difference between the inside and outside of the balloon
$\delta T_{Air}$	temperature difference between the inside and outside of the ballonet

## 1.0 Introduction

Lighter-than-air vehicles usually refer to airships or balloons filled with buoyancy gas to generate static lift, which are also called static lift aerial vehicles [1, 2]. The vertical takeoff and landing capabilities of lighter-than-air vehicles give them an advantage in transporting heavy loads, and their long endurance and long-range motion are attractive for transporting equipment over land or sea areas [3]. Hence, lighter-than-air vehicles have been proposed as environmental monitoring and telecommunication platforms given their high-altitude hovering ability, long-distance displacement and long-term operation [4].

Hanging a load is a convenient way of carrying a payload, allowing for arbitrary placement and exchange of loads; suspended payload can also provide a great view of sensors [5]. However, carrying suspended external loads is a challenging task because the pendulum-like behaviour of slung loads adversely affects aerial vehicles [6]. Therefore, dynamic simulation is important to realise a knowledge-based design to address suspended load swings [7]. This aspect has been extensively studied in the field of helicopters, with different modelling and control methods achieving good suspension performance [8–10].

Compared with helicopters, static lift aerial vehicles have great benefits in the transport of suspended loads, but few theoretical studies exist on the dynamics of lighter-than-air vehicles with slung pods. In the literature, Ardema proposed several buoyant heavy-lift prototypes in 1921 [11], Abdallah established combined kinematic and dynamic models of an airship with a cable-driven parallel robot [12, 13], and Öznur constructed a model of a stratospheric balloon considering transport phenomena and a gas compress–release system [14]. The challenge in accurate altitude control of lighter-than-air vehicles and the uncontrollable horizontal position limit relevant research.

For environmental monitoring, atmospheric experiments require sensor readings across a wide range of altitudes, so autonomous altitude regulation is necessary to change the flight level [15]. Most traditional altitude control methods consider vertical acceleration as control variable, and dynamic equations of altitude with buoyancy have been established [16]. However, the buoyancy of gas is influenced by temperature and pressure variations, which are nonlinear time-varying functions of altitude. To date, no adequate knowledge or data on thermal characteristics are available for establishing an elaborate thermodynamic model of scientific balloons [14, 17, 18]; consequently, accurate altitude control of balloons is difficult.

This paper presents a dynamic model of a high-altitude balloon suspended load system and the dynamic simulation results in the process of altitude control. The general structure of the high-altitude balloon system, which consists of a helium balloon and an air ballonet, is given. The buoyancy is changed by inflating and deflating the ballonet via a two-way blower hanging under the platform. The detailed modelling process of the balloon with suspended load is provided, and an engineering-feasible altitude control system is designed. The dynamic characteristics are analysed during the entire process from autonomous vertical takeoff to different altitude regulations.

## 2.0 Dynamic model of the whole system

### 2.1 System description

The platform consists of the buoyancy body and a pod with mass  $m_p$  connected to the suspension point at the bottom of the buoyancy body by a cable. The structural components of the buoyancy body are similar to those of airships [19], including a helium balloon, a ballonet and a two-way blower. The helium balloon generates buoyancy to balance the platform weight. The two-way blower inflates and deflates the ballonet to regulate the buoyancy to control the descending and ascending processes of the platform, as shown in Fig. 1.

The X-axis of the world coordinate system is supposed to be east–west, and the Z-axis is vertically downward, pointing to the centre of the Earth. The world coordinate system is set parallel to the wind directions to represent the horizontal motion of the platform. The initial state of the body coordinate system  $o_b x_b y_b z_b$  is parallel to the world coordinate system. In a stable flight, the suspension point coordinate system  $o_s x_s y_s z_s$  is always parallel to the body coordinate system and moves down the distance of  $d$ . A model of a high-altitude balloon with slung load is unified into the whole body. After external forces are calculated, all the forces and moments are turned into body frame  $o_b x_b y_b z_b$ , such that the 8-degree of freedom (DOF) differential equations of motion, including two independent DOFs of the pod, are obtained.

### 2.2 Hanging model of the pod in the body frame

#### 2.2.1 Single-point hanging model

The coordinate vector of the suspension point on the balloon in the body coordinate system is  $\mathbf{s} = [0, 0, d]^T$ , where the superscript T represents transposition. With the cable length supposed as  $l$ , at a certain equilibrium position, the angle between the cable and the plane  $o_s y_s z_s$  is defined as the forward angle of inclination  $\theta_L$ , and the angle between the projection of the cable and the  $o_s z_s$  axis of the plane  $o_s x_s z_s$  is defined as the lateral angle of inclination  $\phi_L$ . The position of the pod in the suspension point

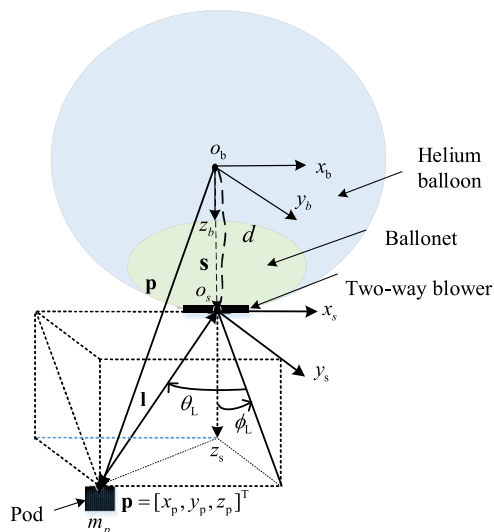


Figure 1. Overall structure and state variables.

coordinate system is  $\mathbf{l} = [-l \sin \theta_L, l \cos \theta_L \sin \phi_L, l \cos \theta_L \cos \phi_L]^T$ . The position vector of the pod in the body coordinate system  $\mathbf{p} = [x_p, y_p, z_p]^T$  is described as

$$\mathbf{p} = \mathbf{l} + \mathbf{s} = [-l \sin \theta_L, l \cos \theta_L \sin \phi_L, l \cos \theta_L \cos \phi_L + d]^T \tag{1}$$

Then, the velocity and acceleration of the pod relative to the body coordinate system are

$$\dot{\mathbf{p}} = \begin{bmatrix} -l \cos \theta_L & 0 \\ -l \sin \theta_L \sin \phi_L & l \cos \theta_L \cos \phi_L \\ -l \sin \theta_L \cos \phi_L & -l \cos \theta_L \sin \phi_L \end{bmatrix} \begin{bmatrix} \dot{\theta}_L \\ \dot{\phi}_L \end{bmatrix} = \mathbf{A}_L \begin{bmatrix} \dot{\theta}_L \\ \dot{\phi}_L \end{bmatrix} \tag{2}$$

$$\begin{aligned} \ddot{\mathbf{p}} &= \begin{bmatrix} -l \cos \theta_L & 0 \\ -l \sin \theta_L \sin \phi_L & l \cos \theta_L \cos \phi_L \\ -l \sin \theta_L \cos \phi_L & -l \cos \theta_L \sin \phi_L \end{bmatrix} \begin{bmatrix} \ddot{\theta}_L \\ \ddot{\phi}_L \end{bmatrix} \\ &+ \begin{bmatrix} l \sin \theta_L \dot{\theta}_L^2 \\ -l \cos \theta_L \sin \phi_L \dot{\theta}_L^2 - 2l \sin \theta_L \cos \phi_L \dot{\phi}_L \dot{\theta}_L - l \cos \theta_L \sin \phi_L \dot{\phi}_L^2 \\ -l \cos \theta_L \cos \phi_L \dot{\theta}_L^2 + 2l \sin \theta_L \sin \phi_L \dot{\phi}_L \dot{\theta}_L - l \cos \theta_L \cos \phi_L \dot{\phi}_L^2 \end{bmatrix} = \mathbf{A}_L \begin{bmatrix} \ddot{\theta}_L \\ \ddot{\phi}_L \end{bmatrix} + \mathbf{B}_L \end{aligned} \tag{3}$$

From Equation (3), because of the constraint with a constant cable length, the pod has two independent state variables:  $\theta_L$  and  $\phi_L$ .

### 2.2.2 Inertial motion of the pod in the body frame

When the body coordinate system has an instantaneous rotating angular velocity  $\boldsymbol{\omega} = [p \ q \ r]^T$ , the position vector  $\mathbf{p}$  produces an entrainment velocity  $\boldsymbol{\omega} \times \mathbf{p}$  represented in the body coordinate system. The motion of the body coordinate system relative to the inertial coordinate system is expressed in the body coordinate system as  $\mathbf{V}_O = [u \ v \ w]^T$ , so the absolute velocity of the pod relative to the inertial coordinate system can be expressed in the body coordinate system as

$$\mathbf{V}_p = \begin{bmatrix} u_p \\ v_p \\ w_p \end{bmatrix} = \mathbf{V}_O + \dot{\mathbf{p}} + \boldsymbol{\omega} \times \mathbf{p} \tag{4}$$

The derivation of this equation gives the expression of the inertial acceleration of the pod in the body coordinate system as

$$\begin{aligned}
 \mathbf{a}_p &= \dot{\mathbf{V}}_p = \dot{\mathbf{V}}_o + \dot{\boldsymbol{\omega}} \times \mathbf{p} + \boldsymbol{\omega} \times \dot{\mathbf{p}} + \boldsymbol{\omega} \times (\mathbf{V}_o + \dot{\mathbf{p}} + \boldsymbol{\omega} \times \mathbf{p}) + \ddot{\mathbf{p}} \\
 &= \begin{bmatrix} \dot{u} \\ \dot{v} \\ \dot{w} \end{bmatrix} + \begin{bmatrix} \dot{p} \\ \dot{q} \\ \dot{r} \end{bmatrix} \times \begin{bmatrix} x_p \\ y_p \\ z_p \end{bmatrix} + \begin{bmatrix} p \\ q \\ r \end{bmatrix} \times \left( \begin{bmatrix} u \\ v \\ w \end{bmatrix} + \begin{bmatrix} p \\ q \\ r \end{bmatrix} \times \begin{bmatrix} x_p \\ y_p \\ z_p \end{bmatrix} \right) + 2 \begin{bmatrix} p \\ q \\ r \end{bmatrix} \times \begin{bmatrix} \dot{x}_p \\ \dot{y}_p \\ \dot{z}_p \end{bmatrix} + \begin{bmatrix} \ddot{x}_p \\ \ddot{y}_p \\ \ddot{z}_p \end{bmatrix} \\
 &= \begin{bmatrix} \dot{u} - vr + wq - x_p(q^2 + r^2) + y_p(pq - \dot{r}) + z_p(pr + \dot{q}) \\ \dot{v} - wp + ur - y_p(p^2 + r^2) + z_p(qr - \dot{p}) + x_p(pq + \dot{r}) \\ \dot{w} - uq + vp - z_p(q^2 + p^2) + x_p(rp - \dot{q}) + y_p(rq + \dot{p}) \end{bmatrix} + 2 \begin{bmatrix} q\dot{z}_p - r\dot{y}_p \\ r\dot{x}_p - p\dot{z}_p \\ p\dot{y}_p - q\dot{x}_p \end{bmatrix} + \begin{bmatrix} \ddot{x}_p \\ \ddot{y}_p \\ \ddot{z}_p \end{bmatrix} \tag{5}
 \end{aligned}$$

where  $\dot{\mathbf{V}}_o + \ddot{\mathbf{p}} + \dot{\boldsymbol{\omega}} \times \mathbf{p} + \boldsymbol{\omega} \times \dot{\mathbf{p}}$  is the inertial acceleration of the pod relative to the origin of the body coordinate system, and  $\boldsymbol{\omega} \times (\mathbf{V}_o + \dot{\mathbf{p}} + \boldsymbol{\omega} \times \mathbf{p})$  is the entrainment acceleration of the body coordinate system relative to the inertial coordinate system.

To simplify the model, this study considers the balloon and the pod to be in steady-state motion, ignoring the product form of the velocity vectors  $\boldsymbol{\omega} \times \dot{\mathbf{p}}$  and  $\boldsymbol{\omega} \times (\mathbf{V}_o + \dot{\mathbf{p}} + \boldsymbol{\omega} \times \mathbf{p})$ . Accordingly,

$$\mathbf{a}_p = \begin{bmatrix} \dot{u} - y_p\dot{r} + z_p\dot{q} \\ \dot{v} - z_p\dot{p} + x_p\dot{r} \\ \dot{w} + -x_p\dot{q} + y_p\dot{p} \end{bmatrix} + \begin{bmatrix} \ddot{x}_p \\ \ddot{y}_p \\ \ddot{z}_p \end{bmatrix} \tag{6}$$

2.2.3 External forces on the body frame

The inertial force on the pod is expressed in the body coordinate system as

$$\mathbf{F}_{pI} = m_p \mathbf{a}_p = \begin{Bmatrix} X_{pI} \\ Y_{pI} \\ Z_{pI} \end{Bmatrix} \tag{7}$$

The gravity of the pod is decomposed into the body coordinate system as

$$\mathbf{F}_{pG} = \begin{Bmatrix} X_{pG} \\ Y_{pG} \\ Z_{pG} \end{Bmatrix} = \begin{Bmatrix} -m_p g \sin \theta \\ m_p g \sin \phi \cos \theta \\ m_p g \cos \phi \cos \theta \end{Bmatrix} \tag{8}$$

The balloon is actively controlled by the buoyancy adjustment system in the vertical direction and floats with the wind in the horizontal direction, so its aerodynamic force is manifested as drag in the vertical direction and as thrust in the horizontal direction. The aerodynamic force on the pod expressed in the body coordinate system is [20]

$$\mathbf{F}_{pA} = \begin{Bmatrix} X_{pA} \\ Y_{pA} \\ Z_{pA} \end{Bmatrix} = \frac{1}{2} \rho S_p C_D (\mathbf{V}_w - \mathbf{V}_p) |\mathbf{V}_w - \mathbf{V}_p| \tag{9}$$

where  $\rho$  is the air density,  $C_D > 0$  is the aerodynamic coefficient of the pod,  $S_p$  is the reference area of the pod, and  $\mathbf{V}_w = [u_w \ v_w \ w_w]^T$  is the wind velocity vector in the body coordinate system.

Under the body coordinate system, the cable force on the pod is  $\mathbf{F}_{pL}$ , which satisfies the force balance on the pod, as shown in Fig. 2.

$$\mathbf{F}_{pA} + \mathbf{F}_{pG} + \mathbf{F}_{pL} = \mathbf{F}_{pI} \tag{10}$$

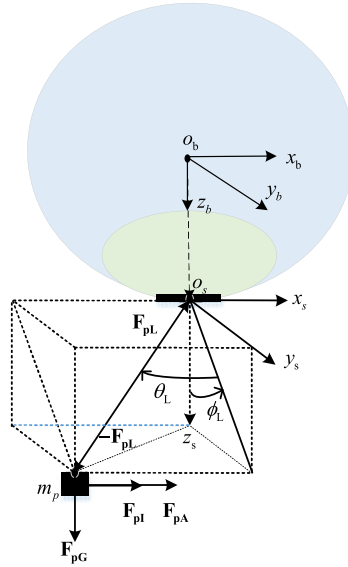


Figure 2. Diagram of the force balance on the pod.

From Equation (10), the pull force  $F_{pL}$  represented in the body coordinate system is

$$\begin{aligned}
 \mathbf{F}_{pL} &= \begin{bmatrix} X_{pL} \\ Y_{pL} \\ Z_{pL} \end{bmatrix} = m_p \begin{bmatrix} \dot{u} - y_p \dot{r} + z_p \dot{q} + \ddot{x}_p \\ \dot{v} - z_p \dot{p} + x_p \dot{r} + \ddot{y}_p \\ \dot{w} - x_p \dot{q} + y_p \dot{p} + \ddot{z}_p \end{bmatrix} - \frac{1}{2} \rho S_p C_D \begin{bmatrix} (u_w - u_p) |u_w - u_p| \\ (v_w - v_p) |v_p - v_w| \\ (w_w - w_p) |w_p - w_w| \end{bmatrix} - m_p g \begin{Bmatrix} -\sin \theta \\ \sin \phi \cos \theta \\ \cos \phi \cos \theta \end{Bmatrix} \\
 &= \begin{cases} m_p (\dot{u} - y_p \dot{r} + z_p \dot{q} + \ddot{x}_p) - \frac{1}{2} \rho S_p C_D (u_w - u_p) |u_w - u_p| + m_p g \sin \theta \\ m_p (\dot{v} - z_p \dot{p} + x_p \dot{r} + \ddot{y}_p) - \frac{1}{2} \rho S_p C_D (v_w - v_p) |v_p - v_w| - m_p g \sin \phi \cos \theta \\ m_p (\dot{w} - x_p \dot{q} + y_p \dot{p} + \ddot{z}_p) - \frac{1}{2} \rho S_p C_D (w_w - w_p) |w_p - w_w| - m_p g \cos \phi \cos \theta \end{cases} \quad (11)
 \end{aligned}$$

Meanwhile, the cable pull force  $F_{pL}$  can be decomposed into the body coordinate system as

$$\mathbf{F}_{pL} = \begin{bmatrix} X_{pL} \\ Y_{pL} \\ Z_{pL} \end{bmatrix} = \|\mathbf{F}_{pL}\|_2 \begin{bmatrix} \sin \theta_L \\ -\sin \phi_L \cos \theta_L \\ -\cos \phi_L \cos \theta_L \end{bmatrix} \quad (12)$$

Equation (12) indicates that two independent equations correspond to two independent state variables, as shown in Equation (3). Through the force balance equation of the pod, we have

$$\begin{cases} X_{pL} \sin \phi_L \cos \theta_L + Y_{pL} \sin \theta_L = 0 \\ Y_{pL} = Z_{pL} \tan \phi_L \end{cases} \quad (13)$$

Equation (11) is substituted into Equation (13), and the mass point motion equation of the pod is obtained as

$$\begin{cases} [m_p (\dot{v} - z_p \dot{p} + x_p \dot{r} + \ddot{y}_p) - \frac{1}{2} \rho S_p C_D (v_w - v_p) |v_p - v_w| - m_p g \sin \phi \cos \theta] \\ = m_p (\dot{w} - x_p \dot{q} + y_p \dot{p} + \ddot{z}_p) - \frac{1}{2} \rho S_p C_D (w_w - w_p) |w_p - w_w| - m_p g \cos \phi \cos \theta \tan \phi_L \\ [m_p (\dot{u} - y_p \dot{r} + z_p \dot{q} + \ddot{x}_p) - \frac{1}{2} \rho S_p C_D (u_w - u_p) |u_p - u_w| + m_p g \sin \theta] \sin \phi_L \cos \theta_L \\ = - [m_p (\dot{v} - z_p \dot{p} + x_p \dot{r} + \ddot{y}_p) - \frac{1}{2} \rho S_p C_D (v_w - v_p) |v_p - v_w| - m_p g \sin \phi \cos \theta] \sin \theta_L \end{cases} \quad (14)$$

**2.3 Thermodynamic model of the buoyancy body**

*2.3.1 Net-lift model in the whole process*

Net-lift is defined here as the lift generated from the helium balloon, which is used to balance the weight of the structure. According to the ideal gas equation, the following relationship exists for the helium balloon, ballonnet and external reference air:

$$\begin{aligned}
 V_{He} &= \frac{m_{He}R_{He}T_{He}}{P_{He}} \\
 \rho_{He} &= \frac{P_{He}}{R_{He}T_{He}}
 \end{aligned}
 \tag{15}$$

$$\begin{aligned}
 V_{Air} &= \frac{m_{Air}R_{Air}T_{Air}}{P_{Air}} \\
 \rho_{Air} &= \frac{P_{Air}}{R_{Air}T_{Air}}
 \end{aligned}
 \tag{16}$$

$$\rho = \frac{P}{R_{Air}T}
 \tag{17}$$

Here,  $R_{Air} = 286.7J/kg/K$  and  $R_{He} = 2078.6J/kg/K$  are the specific gas constants of air and helium, respectively.  $m_{Air}$  and  $m_{He}$  are the internal air mass and helium mass, respectively.  $\rho_{Air}$  and  $\rho_{He}$  are the internal air density and helium density, respectively;  $T_{He}$  and  $T_{Air}$  are the helium temperature and internal air temperature, respectively;  $P_{He}$  and  $P_{Air}$  are the helium balloon pressure and internal air ballonnet pressure, respectively;  $V_{He}$  and  $V_{Air}$  are the helium balloon volume and ballonnet volume, respectively. The total volume of the buoyancy body is obtained as  $V = V_{Air} + V_{He}$ . Given the density  $\rho$ , pressure  $P$  and temperature  $T$  of the external reference atmosphere, the net-lift from the buoyancy of the helium balloon is modelled as [20]

$$\begin{aligned}
 L_{He} &= g\rho V_{He} - m_{He}g + g\rho V_{Air} - m_{Air}g \\
 &= m_{He}g \left( \frac{\rho V_{He}}{m_{He}} - 1 \right) + m_{Air}g \left( \frac{\rho V_{Air}}{m_{Air}} - 1 \right) \\
 &= m_{He}g \left( \frac{\frac{PM_{Air}}{RT} \frac{m_{He}RT_{He}}{P_{He}M_{He}}}{m_{He}} - 1 \right) + m_{Air}g \left( \frac{\frac{PM_{Air}}{RT} \frac{m_{Air}RT_{Air}}{P_{Air}M_{Air}}}{m_{Air}} - 1 \right) \\
 &= m_{He}g \left( \frac{M_{Air}}{M_{He}} \frac{P}{P_{He}} \frac{T_{He}}{T} - 1 \right) + m_{Air}g \left( \frac{P}{P_{Air}} \frac{T_{Air}}{T} - 1 \right) \\
 &= m_{He}g \left( \frac{M_{Air}}{M_{He}} \frac{P}{P + (P_{He} - P)} \frac{T + (T_{He} - T)}{T} - 1 \right) + m_{Air}g \left( \frac{P}{P + (P_{Air} - P)} \frac{T + (T_{Air} - T)}{T} - 1 \right)
 \end{aligned}
 \tag{18}$$

Here, the universal gas constant  $R = 8.314J/K/mol$ .  $M_{Air}$  and  $M_{He}$  are the molar masses of air and helium, respectively.  $\delta T_{He} = T_{He} - T$  and  $\delta T_{Air} = T_{Air} - T$  are the temperature difference between the inside and outside of the helium balloon and ballonnet, respectively.  $\delta P_{He} = P_{He} - P$  and  $\delta P_{Air} = P_{Air} - P$  stand for the pressure difference between the inside and outside of the helium balloon and ballonnet, respectively. In general,  $\frac{P_{He}-P}{P}$  and  $\frac{P_{Air}-P}{P}$  are small at low altitude, but they cannot be ignored when the balloon is approaching the climb ceiling.

For zero-pressure balloons [21], no overpressure occurs, so net-lift is simplified as

$$L_{He} = m_{He}g \left( \frac{M_{Air}}{M_{He}} \frac{T + (T_{He} - T)}{T} - 1 \right) + m_{Air}g \left( \frac{T + (T_{Air} - T)}{T} - 1 \right)
 \tag{19}$$

Here,  $\frac{T_{He}-T}{T}$  and  $\frac{T_{Air}-T}{T}$  depend on the thermal characteristics of the balloon, as will be described in the following section.

For balloon long-time flying at a stable altitude,  $\delta T_{He}$  and  $\delta T_{Air}$  are neglected, then the net-lift becomes

$$L_{He} = m_{He}g \left( \frac{M_{Air}}{M_{He}} \frac{P}{P + (P_{He} - P)} - 1 \right) + m_{Air}g \left( \frac{P}{P + (P_{Air} - P)} - 1 \right) \tag{20}$$

2.3.2 Thermodynamic models during ascending and descending

During the ascending process, the balloon is not full of gas. Thus, the pressure of the helium balloon is [20]

$$\begin{aligned} P_{He} &= P = g\rho z \\ \Rightarrow \frac{dP_{He}}{dz} &= \frac{dP}{dz} = -g\rho = -g \frac{PM_{Air}}{RT} \\ \Rightarrow \frac{dP_{He}}{P_{He}dz} &= \frac{dP}{Pd z} = -g \frac{M_{Air}}{RT} \end{aligned} \tag{21}$$

where  $M_{Air}$  is the molar mass of air. The thermal environment of the high-altitude balloon includes the internal and external environments. The heat transfer between the high-altitude balloon and external air involves radiation and the convection amongst the film, internal gases and external air. In consideration of the semitransparent property of the film, the thermal radiation amongst the film, external reference air and internal gases includes direct solar irradiation, reflected and scattered solar radiation and infrared radiation. Given that the film is very thin, its heat conduction is neglected for simplification. In accordance with the first law of thermodynamics, energy conservation equations for the helium balloon and the internal air ballonet are established as follows [19]:

$$\begin{aligned} m_{He}C_{p,He} \frac{dT_{He}}{dt} &= \sum Q_{He,i} + V_{He} \frac{dP_{He}}{dt} \\ m_{Air}C_{p,Air} \frac{dT_{Air}}{dt} &= \sum Q_{Air,i} + V_{Air} \frac{dP_{Air}}{dt} \text{ (ascending)} \\ m_{Air}C_{p,Air} \frac{dT_{Air}}{dt} &= \sum Q_{Air,i} + V_{Air} \frac{dP_{Air}}{dt} + C_{p,Air}(T_{Air} - T) \frac{dm_{Air}}{dt} \text{ (descending)} \end{aligned} \tag{22}$$

where  $C_{p,He}$  and  $C_{p,Air}$  are the specific heat of helium and air at constant pressure, respectively.  $\sum Q_{He,i}$  and  $\sum Q_{Air,i}$  represent the heat transfer rate of helium and internal air with the environment, respectively. Equation (22) represents the energy conservation of helium and internal air. Specifically, the second equation is for the ascending phase, and the third one is for the descending phase, which considers the added heat from the pumped external air. The pump inflates the balloon by doing work, thereby generating heat. When deflating, the blower is driven by the internal and external pressure difference, and the energy required is negligible.

The heat transfer rate considered in Equation (22) includes the solar radiation heat  $IaA_1$ , the convective heat transferred between internal air and reference air  $K_1A_2 (T - (T_{He}V_{He} + T_{Air}V_{Air}) / V)$  and the heat transferred between internal air and helium  $K_2A_3 (T_{He} - T_{Air})$ , as shown below:

$$\begin{aligned} \sum Q_{He,i} &= (K_1A_2 (T - (T_{He}V_{He} + T_{Air}V_{Air}) / V) + IaA_1)V_{He}/V + K_2A_3 (T_{Air} - T_{He}) \\ \sum Q_{Air,i} &= (K_1A_2 (T - (T_{He}V_{He} + T_{Air}V_{Air}) / V) + IaA_1)V_{Air}/V + K_2A_3 (T_{He} - T_{Air}) \end{aligned} \tag{23}$$

Here,  $I = 1367W/m^2$  is the estimated solar constant,  $a = 0.4$  is the estimated efficiency of absorbing radiation, and  $A_1 = V^{2/3}$  is the estimated effective area of absorbing radiation.  $K_1 = 30W/(m^2K)$  and  $A_2 = V^{2/3}$  are the estimated heat transfer coefficient and the heat transfer area between the balloon and



the environment, respectively.  $K_2 = 10W/(m^2K)$  and  $A_3 = V_{Air}^{2/3}$  are the estimated heat transfer coefficient and the heat transfer area between **internal air and helium, respectively**.

From Equations (15) and (21), we have

$$\begin{aligned} V_{He} \frac{dP_{He}}{dt} &= m_{He} R_{He} T_{He} \frac{dP_{He}}{P_{He}} \frac{dz}{dt} \\ &= -gm_{He} R_{He} T_{He} \frac{M_{Air}}{R_{Air} T} \dot{z} \\ &= -gm_{He} \frac{R_{He} T_{He}}{R_{Air} T} \dot{z} \end{aligned} \tag{24}$$

Accordingly, we obtain

$$m_{He} C_{p,He} \frac{dT_{He}}{dt} = \sum Q_{He,i} - gm_{He} \frac{R_{He} T_{he}}{RT} \dot{z} \tag{25}$$

The current temperature of helium with vertical motion can be calculated using Equation (25), and the total net-lift can be determined via Equation (19).

2.3.3 *Overpressure models with fixed volume ratio*

When the balloon reaches the maximum altitude of 20km, a pressure difference  $\delta P_{Air}$  occurs between the inside and outside of the balloon. Thus, the balloon has a fixed shape, and its volume is at the maximum value. This condition is defined as the steady state of the balloon. The pressure differences of the helium balloon and the ballonnet are assumed to be equal, i.e.  $\delta P_{Air} = \delta P_{He}$ , under the steady state for a given station-keeping altitude, which means that the shape will not change during the height adjustment process. The temperature difference between inside and outside the sphere for a long time at one altitude is ignored. For the mass conservation, we have

$$\begin{aligned} m_{Air} &= \rho V_{Air} \left( 1 + \frac{\delta P_{Air}}{P} \right) \\ m_{He} &= \rho_{He0} V_{He} \left( 1 + \frac{\delta P_{He}}{P} \right) \\ V &= V_{Air} + V_{He} \end{aligned} \tag{26}$$

where  $\rho_{He0}$  is the helium density under a normal pressure. For the balloon in a steady state, the volume ratio  $k$  of the helium balloon to the ballonnet is fixed and can be deduced as

$$\begin{aligned} k &= \frac{V_{He}}{V_{Air}} = \frac{m_{He} \rho_{Air0}}{m_{Air} \rho_{He0}} \\ V_{Air} &= V/(1+k) \\ V_{He} &= V - V_{Air} \end{aligned} \tag{27}$$

For a stable balance at any altitude, the balloon has a vertical balance, i.e.

$$\begin{cases} g[(\rho - \rho_{He0})V_{He} - \rho_{He0} \frac{\delta \rho_{He}}{P} V_{He} - \rho \frac{\delta P_{Air}}{P} V_{Air}] \Big|_h - (m_{struc} + m_p)g = 0 \\ V_{He} + V_{Air} = V \end{cases} \tag{28}$$

where  $m_{struc}$  is the mechanical structure mass, mainly including the two-way blower and the envelope.

The net-lift generated in Equation (28) is another form of Equation (20). If we substitute Equation (26) into Equation (28), the following relationship exists:  $\rho = \rho_{He0} \frac{M_{Air}}{M_{He}}$ .

2.4 Dynamic model of the overall system

2.4.1 Nonlinear model

From Equation (11), the force and moment generated by the cable pull force on the balloon expressed in the body coordinate system are

$$\left\{ \begin{aligned} -\mathbf{F}_{pL} &= \begin{cases} -m_p(\dot{u} - y_p\dot{r} + z_p\dot{q} + \ddot{x}_p) + \frac{1}{2}\rho S_p C_D(u_w - u_p) |u_w - u_p| - m_p g \sin \theta \\ -m_p(\dot{v} - z_p\dot{p} + x_p\dot{r} + \ddot{y}_p) + \frac{1}{2}\rho S_p C_D(v_w - v_p) |v_w - v_p| + m_p g \sin \phi \cos \theta \\ -m_p(\dot{w} - x_p\dot{q} + y_p\dot{p} + \ddot{z}_p) + \frac{1}{2}\rho S_p C_D(w_w - w_p) |w_w - w_p| + m_p g \cos \phi \cos \theta \end{cases} \\ -\mathbf{s} \times \mathbf{F}_{pL} &= \begin{cases} -d[-m_p(\dot{v} - z_p\dot{p} + x_p\dot{r} + \ddot{y}_p) + \frac{1}{2}\rho S_p C_D(v_w - v_p) |v_w - v_p| + m_p g \sin \phi \cos \theta] \\ d[-m_p(\dot{u} - y_p\dot{r} + z_p\dot{q} + \ddot{x}_p) + \frac{1}{2}\rho S_p C_D(u_w - u_p) |u_w - u_p| - m_p g \sin \theta] \\ 0 \end{cases} \end{aligned} \right. \tag{29}$$

where  $\phi$ ,  $\theta$  and  $\psi$  are the Euler angles of the body in the world coordinate system.

The dynamics of the balloon considering the cable pull force is

$$\left\{ \begin{aligned} X_a - mg \sin \theta - X_{pL} &= m(\dot{u} - vr + wq) \\ Y_a + mg \cos \theta \sin \phi - Y_{pL} &= m(\dot{v} - wp + ur) \\ Z_a + mg \cos \theta \cos \phi - Z_{pL} - B &= m(\dot{w} - uq + vp) \\ L_a + dY_{pL} &= I_x\dot{p} + (I_z - I_y)r q \\ M_a - dX_{pL} &= I_y\dot{q} + (I_x - I_z)r p \\ N_a &= I_z\dot{r} \end{aligned} \right. \tag{30}$$

where the total mass of the balloon  $m = m_{Air} + m_{He} + m_{stru} + m_{add}$ ; here,  $m_{add}$  is the additional mass [20].  $I_x$ ,  $I_y$  and  $I_z$  are the inertial moments,  $\rho$  is the density of the reference air,  $Q$  is the dynamic pressure, and  $B = \rho V$  is the total buoyancy.  $X_a = \frac{1}{2}\rho S C_X(u_w - u) |u_w - u|$ ,  $Y_a = \frac{1}{2}\rho S C_Y(v_w - v) |v_w - v|$  and  $Z_a = \frac{1}{2}\rho S C_Z(w_w - w) |w_w - w|$  are the aerodynamic components of the balloon along the three axes of the body coordinate system.  $L_a = Q S l_{ref} C_l$ ,  $M_a = Q S l_{ref} C_m$  and  $N_a = Q S l_{ref} C_n$  are the aerodynamic moment components of the three axes around the body coordinate system.  $C_X$ ,  $C_Y$ ,  $C_Z$ ,  $C_l$ ,  $C_m$  and  $C_n$  are the aerodynamic coefficients of the balloon,  $S$  is the reference area, and  $l_{ref}$  is the reference length of the balloon.

Equations (14) and (30) constitute the whole 8-DOF system dynamics, i.e.

$$\left\{ \begin{aligned} &[m_p(\dot{v} - z_p\dot{p} + x_p\dot{r} + \ddot{y}_p) - \frac{1}{2}\rho S_p C_D(v_w - v_p) |v_p - v_w| - m_p g \sin \phi \cos \theta] \\ &= [m_p(\dot{w} - x_p\dot{q} + y_p\dot{p} + \ddot{z}_p) - \frac{1}{2}\rho S_p C_D(w_w - w_p) |w_p - w_w| - m_p g \cos \phi \cos \theta] \text{tg} \phi_L \\ &[m_p(\dot{u} - y_p\dot{r} + z_p\dot{q} + \ddot{x}_p) - \frac{1}{2}\rho S_p C_D(u_w - u_p) |u_p - u_w| + m_p g \sin \theta] \sin \phi_L \cos \theta_L \\ &= -[m_p(\dot{v} - z_p\dot{p} + x_p\dot{r} + \ddot{y}_p) - \frac{1}{2}\rho S_p C_D(v_w - v_p) |v_p - v_w| - m_p g \sin \phi \cos \theta] \sin \theta_L \\ &m(\dot{u} - vr + wq) = X_a - mg \sin \theta - m_p(\dot{u} - y_p\dot{r} + z_p\dot{q} + \ddot{x}_p) + \frac{1}{2}\rho S_p C_D(u_w - u_p) |u_w - u_p| - m_p g \sin \theta \\ &m(\dot{v} - wp + ur) = Y_a + mg \cos \theta \sin \phi - m_p(\dot{v} - z_p\dot{p} + x_p\dot{r} + \ddot{y}_p) + \frac{1}{2}\rho S_p C_D(v_w - v_p) |v_p - v_w| \\ &\quad + m_p g \sin \phi \cos \theta \\ &m(\dot{w} - uq + vp) = Z_a + mg \cos \theta \cos \phi - m_p(\dot{w} - x_p\dot{q} + y_p\dot{p} + \ddot{z}_p) + \frac{1}{2}\rho S_p C_D(w_w - w_p) |w_p - w_w| \\ &\quad + m_p g \cos \phi \cos \theta - B \\ &I_x\dot{p} + (I_z - I_y)r q = L_a + d(m_p(\dot{v} - z_p\dot{p} + x_p\dot{r} + \ddot{y}_p) - \frac{1}{2}\rho S_p C_D(v_w - v_p) |v_p - v_w| - m_p g \sin \phi \cos \theta) \\ &I_y\dot{q} + (I_x - I_z)r p = M_a - d(m_p(\dot{u} - y_p\dot{r} + z_p\dot{q} + \ddot{x}_p) - \frac{1}{2}\rho S_p C_D(u_w - u_p) |u_w - u_p| + m_p g \sin \theta) \\ &I_z\dot{r} = N_a \end{aligned} \right. \tag{31}$$

Equation (31) can be rearranged into

$$\left\{ \begin{aligned}
 & m_p \dot{v} - m_p \operatorname{tg} \phi_L \dot{w} - (m_p z_p + m_p \operatorname{tg} \phi_L y_p) \dot{p} + m_p \operatorname{tg} \phi_L x_p \dot{q} + m_p x_p \dot{r} + m_p \ddot{y}_p - m_p \operatorname{tg} \phi_L \ddot{z}_p \\
 &= \frac{1}{2} \rho S_p C_D (v_w - v_p) |v_p - v_w| + m_p g \sin \phi \cos \theta - \frac{1}{2} \rho S_p C_D (w_w - w_p) |w_p - w_w| \operatorname{tg} \phi_L \\
 &\quad - m_p g \cos \phi \cos \theta \operatorname{tg} \phi_L \\
 & m_p \sin \phi_L \cos \theta_L \dot{u} - m_p \sin \theta_L \dot{v} - m_p z_p \sin \theta_L \dot{p} - (m_p y_p \sin \phi_L \cos \theta_L - m_p x_p \sin \theta_L) \dot{r} + m_p z_p \sin \phi_L \cos \theta_L \dot{q} \\
 &\quad + m_p \sin \phi_L \cos \theta_L \ddot{x}_p + m_p \sin \theta_L \ddot{y}_p \\
 &= \frac{1}{2} \rho S_p C_D (u_w - u_p) |u_p - u_w| \sin \phi_L \cos \theta_L - m_p g \sin \theta \sin \phi_L \cos \theta_L + \frac{1}{2} \rho S_p C_D (v_w - v_p) |v_p - v_w| \sin \theta_L \\
 &\quad + m_p g \sin \phi \cos \theta \sin \theta_L \\
 & (m + m_p) \dot{u} + m_p z_p \dot{q} - m_p y_p \dot{r} + m_p \ddot{x}_p = X_a + \frac{1}{2} \rho S_p C_D (u_w - u_p) |u_w - u_p| - (mg + m_p g - B) \sin \theta \\
 &\quad + mvr - mwq \\
 & (m + m_p) \dot{v} - m_p z_p \dot{p} + m_p x_p \dot{r} + m_p \ddot{y}_p = Y_a + \frac{1}{2} \rho S_p C_D (v_w - v_p) |v_p - v_w| + (mg + m_p g - B) \sin \phi \cos \theta \\
 &\quad + mwp - mur \\
 & (m + m_p) \dot{w} + m_p y_p \dot{p} - m_p x_p \dot{q} + m_p \ddot{z}_p = Z_a + \frac{1}{2} \rho S_p C_D (w_w - w_p) |w_p - w_w| \\
 &\quad + (mg + m_p g - B) \cos \phi \cos \theta \operatorname{mu}q - mvp \\
 & -m_p d \dot{v} + (I_x + m_p dz_p) \dot{p} - m_p dx_p \dot{r} - m_p d \ddot{y}_p = L_a - d \frac{1}{2} \rho S_p C_D (v_w - v_p) |v_p - v_w| - (mg z_g \\
 &\quad + (d + z_p) m_p g) \sin \phi \cos \theta - (I_z - I_y) r q \\
 & m_p d \dot{u} + (I_y + m_p dz_p) \dot{q} - m_p dy_p \dot{r} + m_p d \ddot{x}_p = M_a + d \frac{1}{2} \rho S_p C_D (u_w - u_p) |u_w - u_p| - (mg z_g \\
 &\quad + (d + z_p) m_p g) \sin \theta - (I_x - I_z) r p \\
 & I_z \dot{r} = N_a
 \end{aligned} \right. \tag{32}$$

2.4.2 Point mass model

The balloon is assumed to be stable in level flight, such that the movement of the pod is balanced. The changes in the angular velocity and acceleration of the balloon are ignored; thus,  $p = q = r = 0$ , and  $\dot{p} = \dot{q} = \dot{r} = 0$ . The point mass model of the platform is simplified to

$$\left\{ \begin{aligned}
 & m_p \dot{v} + m_p \ddot{y}_p - m_p \operatorname{tg} \phi_L \dot{w} - m_p \operatorname{tg} \phi_L \ddot{z}_p = -\frac{1}{2} \rho S_p C_D (w_w - w_p) |w_p - w_w| \operatorname{tg} \phi_L - m_p g \operatorname{tg} \phi_L \\
 &\quad + \frac{1}{2} \rho S_p C_D (v_w - v_p) |v_p - v_w| \\
 & m_p \sin \phi_L \cos \theta_L \dot{u} + m_p \sin \phi_L \cos \theta_L \ddot{x}_p + m_p \sin \theta_L \dot{v} + m_p \sin \theta_L \ddot{y}_p \\
 &= \frac{1}{2} \rho S_p C_D (u_w - u_p) |u_p - u_w| \sin \phi_L \cos \theta_L + \frac{1}{2} \rho S_p C_D (v_w - v_p) |v_p - v_w| \sin \theta_L \\
 & m \dot{u} + m_p (\dot{u} + \ddot{x}_p) = \frac{1}{2} \rho S C_X (u_w - u) |u - u_w| + \frac{1}{2} \rho S_p C_D (u_w - u_p) |u_p - u_w| - mg \sin \theta - m_p g \sin \theta \\
 & m \dot{v} + m_p (\dot{v} + \ddot{y}_p) = \frac{1}{2} \rho S C_Y (v_w - v) |v - v_w| + \frac{1}{2} \rho S_p C_D (v_w - v_p) |v_p - v_w| + mg \cos \theta \sin \phi \\
 &\quad + m_p g \sin \phi \cos \theta \\
 & m \dot{w} + m_p (\dot{w} + \ddot{z}_p) = \frac{1}{2} \rho S C_Z (w_w - w) |w - w_w| + \frac{1}{2} \rho S_p C_D (w_w - w_p) |w_p - w_w| + mg \cos \theta \cos \phi \\
 &\quad + m_p g \cos \phi \cos \theta - B
 \end{aligned} \right. \tag{33}$$

Equation (3) is combined with Equation (33) to form the kinetic equation of the mass point system.

2.4.3 Static equilibrium

This study assumes that the platform is stable in level flight and that the pod is statically balanced; hence,  $p = q = r = 0$ ,  $\dot{p} = \dot{q} = \dot{r} = 0$ ,  $\dot{u} = \dot{v} = \dot{w} = 0$  and  $\ddot{x}_p = \ddot{y}_p = \ddot{z}_p = 0$  hold. Then, the cable pull force is simplified to

$$\mathbf{F}_{pL} = \begin{bmatrix} -\frac{1}{2} \rho S_p C_D (u_w - u_p) |u_p - u_w| + m_p g \sin \theta \\ -\frac{1}{2} \rho S_p C_D (v_w - v_p) |v_p - v_w| - m_p g \sin \phi \cos \theta \\ -\frac{1}{2} \rho S_p C_D (w_w - w_p) |w_p - w_w| - m_p g \cos \phi \cos \theta \end{bmatrix} \tag{34}$$

The platform is in a static equilibrium state, so

$$\begin{cases} \frac{1}{2} \rho S C_X (u_w - u) |u - u_w| + \frac{1}{2} \rho S_p C_D (u_w - u_p) |u_p - u_w| = 0 \\ \frac{1}{2} \rho S C_Y (v_w - v) |v - v_w| + \frac{1}{2} \rho S_p C_D (v_w - v_p) |v_p - v_w| = 0 \\ \frac{1}{2} \rho S C_Z (w_w - w) |w - w_w| + \frac{1}{2} \rho S_p C_D (w_w - w_p) |w_p - w_w| + mg + m_p g - B = 0 \\ -\frac{1}{2} \rho S_p C_D (w_w - w_p) |w_p - w_w| \operatorname{tg} \phi_L + \frac{1}{2} \rho S_p C_D (v_w - v_p) |v_p - v_w| - m_p g \operatorname{tg} \phi_L \\ \frac{1}{2} \rho S_p C_D (u_w - u) |u - u_w| \sin \phi_L \cos \theta_L + \frac{1}{2} \rho S_p C_D (v_w - v_p) |v_p - v_w| \sin \theta_L \end{cases} \tag{35}$$

Supposing that the attitude of the helium balloon is negligible, i.e.  $\theta = \phi = 0$ , this study further simplifies the cable pull force to

$$\mathbf{F}_{pL} = \begin{bmatrix} -\frac{1}{2} \rho S_p C_D (u_w - u_p) |u_p - u_w| \\ -\frac{1}{2} \rho S_p C_D (v_w - v_p) |v_p - v_w| \\ -\frac{1}{2} \rho S_p C_D (w_w - w_p) |w_p - w_w| - m_p g \end{bmatrix} \tag{36}$$

When the moving speed of the pod and the wind speed are equal, the horizontal component of the cable pull force of the platform is zero. The vertical component of the cable pull force is the magnitude of the pod weight. Hence, the pod static balance is simplified to

$$\begin{cases} \frac{1}{2} \rho S_p C_D (v_w - v_p) |v_p - v_w| = [\frac{1}{2} \rho S_p C_D (w_w - w_p) |w_p - w_w| + m_p g] \operatorname{tg} \phi_L \\ \frac{1}{2} \rho S_p C_D (u_w - u) |u - u_w| \sin \phi_L \cos \theta_L + \frac{1}{2} \rho S_p C_D (v_w - v_p) |v_p - v_w| \sin \theta_L = 0 \end{cases} \tag{37}$$

Under this condition, the hanging angle of the pod satisfies the following equation:

$$\begin{cases} \phi_L = \operatorname{atg} \left( \frac{\frac{1}{2} \rho S_p C_D (v_w - v_p) |v_p - v_w|}{\frac{1}{2} \rho S_p C_D (w_w - w_p) |w_p - w_w| + m_p g} \right) \text{ or } \phi_L = \operatorname{atg} \left( \frac{Y_{pL}}{Z_{pL}} \right) \\ \theta_L = \operatorname{atg} \left( \frac{-(u_w - u) |u - u_w| \sin \phi_L}{(v_w - v_p) |v_p - v_w|} \right) \text{ or } \theta_L = \operatorname{atg} \left( \frac{-X_{pL}}{\sqrt{Y_{pL}^2 + Z_{pL}^2}} \right) \end{cases} \tag{38}$$

**Table 1.** *Parameters of the platform*

Parameters	Value
Initial altitude	10m
Diameter of the balloon	15m
Cable length	7.5m
Initial position of the pod	(0,0,14.5)m
Gravity centre	(0,0,4)m
Total volume of the balloon	1,280m <sup>3</sup>
Initial helium mass	15.5kg
Initial ballonnet mass	5.546kg
Helium volume at 10m	91.82m <sup>3</sup>
Ballonnet volume at 10m	4.5317m <sup>3</sup>
Residual pressure difference at 20km altitude	200Pa
Maximum pressure difference of the platform	500Pa
Structural mass $m_{struc}$	62.7kg
Pod mass $m_p$	30kg
Buoyancy at 10m altitude	96.875kg
Lift at 10m altitude	4.1164kg
Maximum flow rate of the blower	0.5kg/s
Pressure difference change threshold $\delta$	20Pa/s

From Equation (38), the lateral angle of inclination  $\phi_L$  is determined by the ratio of the lateral force to the vertical component force experienced by the pod. The forward angle of inclination  $\theta_L$  is determined by the ratio of the forward force experienced by the pod to the resultant force in the plane  $o_s x_s y_s z_s$ .

### 3.0 Differential pressure difference-based altitude adjustment

#### 3.1 Overall parameter design

The platform parameters are designed for the task of environmental monitoring. The designed hover altitude of 20km is the optimal altitude for high-altitude balloons when the wind field is considered; 20km is the bottom of the stratosphere, which is a low wind zone. The vertical mixing motion of the atmosphere is weak, and the atmospheric motion is mostly horizontal, which is convenient for position control of the balloon. The platform's maximum hovering altitude is supposed to be 20km, and the structural mass is  $m_{struc} = 63\text{kg}$ . The pressure difference at 20km is designed to be  $\delta P_{Air} = \delta \rho_{He} = 200\text{Pa}$ . The maximum pressure difference for the envelope to withstand is  $\Delta P_{max} = 500\text{Pa}$ . The diameter of this platform is about 15m, and the overall volume is about  $V = 1280\text{m}^3$ . The lift and gravity balance at 20km and the total volume are assumed to remain the same during the altitude adjustment process. The helium mass at 20km is 15.5kg.

The parameters of the platform and the calculation results at 20km for balance are shown in Table 1.

This study assumes that no gas exchange occurs during the ascent process. Thus, at the initial altitude of 10m, the helium mass and air mass are the same as those at 20km altitude. Then, the total vertical force obtained at 10m is 4.1164kg, which reaches the initial ascent.

#### 3.2 General controller structure

Complex controller algorithms are unsuitable for engineering applications because achieving an accurate dynamic model is difficult, so this study proposes an altitude adjustment method based on differential pressure difference. This controller design is simply implemented by avoiding the trouble

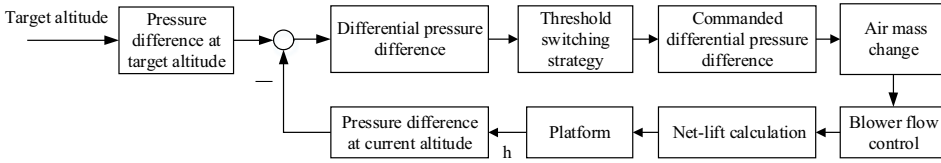


Figure 3. General structure of the controller.

of accurate modelling, and it is convenient for adoption in practical controller design. The controller structure is shown in Fig. 3.

The pressure difference  $\delta P_{He,t} = \delta P_{Air,t}$  at the target altitude and the pressure difference  $\delta P_{He,c} = \delta P_{Air,c}$  at the current altitude can be deduced from the lift and weight balance condition at different altitudes given in Equation (28), as shown as follows:

$$\delta P_{He,t} = \delta P_{Air,t} = \left. \frac{[(\rho_{Air0} - \rho_{He0})V_{He} - (m_{struc} + m_p)]P}{\rho_{He0}V_{He} + \rho_{Air0}V_{Air}} \right|_{h=targetaltitude} \tag{39}$$

$$\delta P_{He,h} = \delta P_{Air,h} = \left. \frac{[(\rho_{Air0} - \rho_{He0})V_{He} - (m_{struc} + m_p)]P}{\rho_{He0}V_{He} + \rho_{Air0}V_{Air}} \right|_{h=currentaltitude} \tag{40}$$

The differential pressure difference between the current and target altitudes is calculated as

$$\Delta = \delta P_{Air,h} - \delta P_{Air,t} \tag{41}$$

The pressure difference-based threshold switching strategy is shown in Fig. 4.

Given that the altitude is regulated through the inflation or deflation of the ballonet by the two-way blower, the commanded tracking pressure difference of the ballonet  $\delta P_{Air,c}$  is determined by  $\Delta$  via a threshold switching strategy.  $\Delta$  is compared with a pressure difference change threshold  $\delta$ , which is defined in the system design phase. The two-way blower provides the maximum air mass change per control cycle for inflation and deflation, which is the design basis for  $\delta$ . For this platform, the control period is set to 1 s, and  $\delta=20\text{Pa/s}$ . The maximum flow rate of the blower is lower than 0.5kg/s at an arbitrary altitude, as decided and validated from subsequent simulations.

If  $\Delta$  is less than  $\delta$ , then the target pressure difference is assigned directly to the tracking pressure difference ; if  $\Delta$  exceeds  $\delta$ , then the tracking pressure difference is the current pressure difference plus or minus the threshold  $\delta$  depending on the sign of  $\Delta$ . The tracking commanded pressure difference assignment logic is as follows:

$$\begin{cases} \delta P_{Air,c} = \delta P_{Air,t} & |\Delta| < \delta \\ \delta P_{Air,c} = \delta P_{Air,h} - \delta & \Delta > \delta \\ \delta P_{Air,c} = \delta P_{Air,h} + \delta & \Delta < -\delta \end{cases} \tag{42}$$

On the basis of the condition that the pressure difference between the helium balloon and the ballonet is equal, i.e.  $\delta P_{He,c} = \delta P_{Air,c}$ , only the ballonet has gas exchange during the altitude adjustment process, and the required helium balloon volume is calculated through the conservation of helium mass. Then, the ballonet volume is derived from the invariant total volume. From helium mass conservation, the following equation can be derived:

$$\begin{aligned} V_{He,c} &= \frac{m_{He}}{\rho_{He0} \left(1 + \frac{\delta P_{He,c}}{P}\right)} \\ V_{Air,c} &= V - V_{He,c} \end{aligned} \tag{43}$$

where  $V_{He,c}$  and  $V_{Air,c}$  are the commanded volumes to be reached.

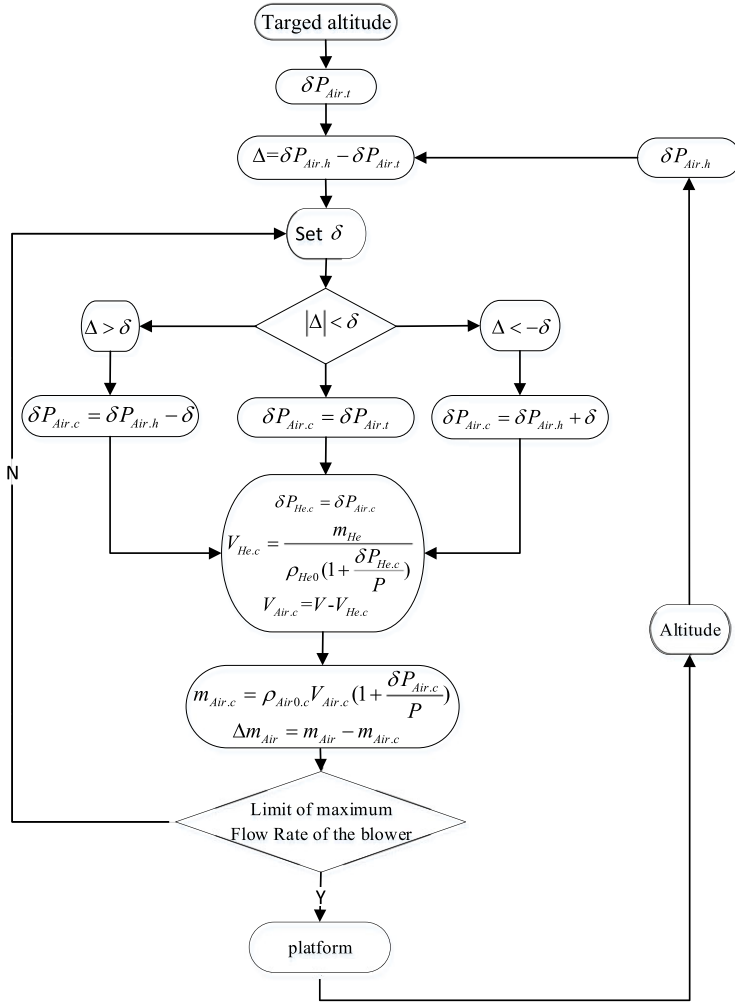


**Figure 4.** Differential pressure difference-based threshold switching strategy.

The remaining air mass of the ballonnet at any control period should satisfy the commanded volume and commanded tracking pressure difference, i.e.

$$m_{Air,c} = \rho_{Air0,c} V_{Air,c} \left( 1 + \frac{\delta P_{Air,c}}{P} \right) \tag{44}$$

The required mass change of the ballonnet is calculated as

$$\Delta m_{Air} = m_{Air} - m_{Air,c} \tag{45}$$

The two-way blower realises the inflation and deflation of the ballonnet and achieves these air mass changes by controlling the size of the blower flow, which should satisfy the flow rate of the blower at any altitude.

In this scheme, the control strategy can be worked out even without access to an accurate dynamic model. Only the pressure difference at different altitudes needs to be determined. The commanded pressure difference in Equation (39) is decided by the volume ratio, atmospheric density and pressure at the target altitude. The volume ratio  $k$  at the target altitude is undetermined, so the volume ratio at the current altitude in Equation (40) is used to calculate the ballonnet volume  $V_{Air,t}$  and the helium balloon

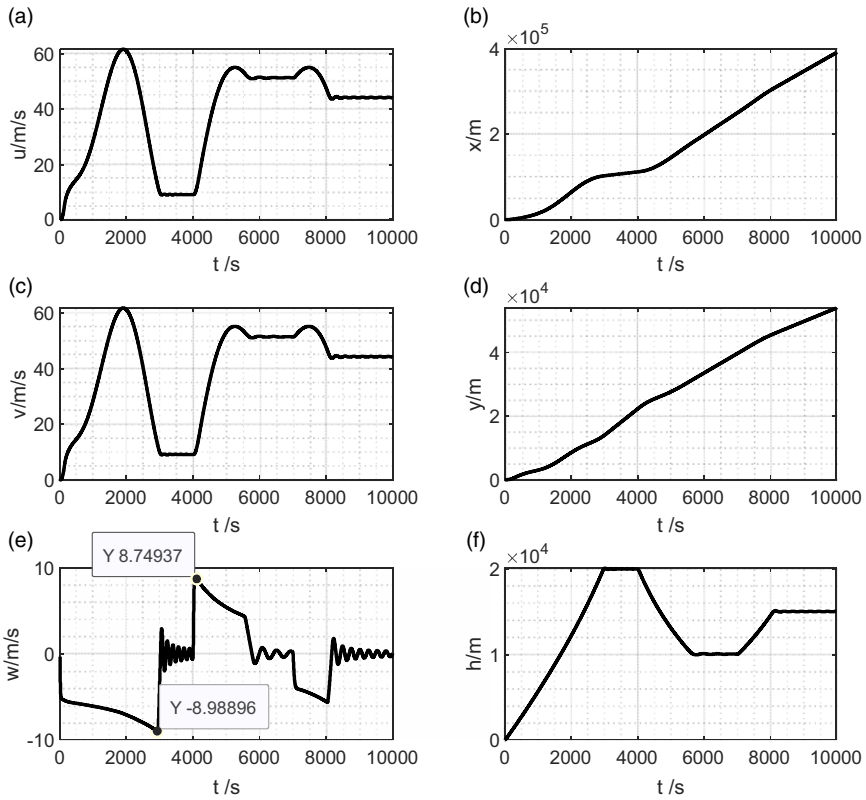


Figure 5. Velocities and positions of the platform.

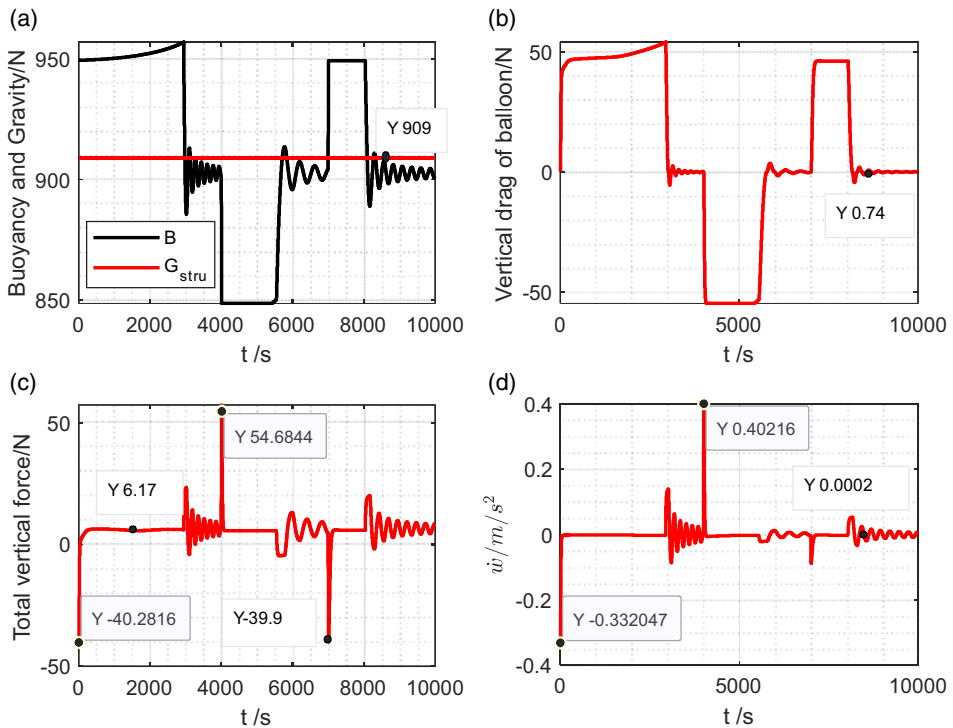
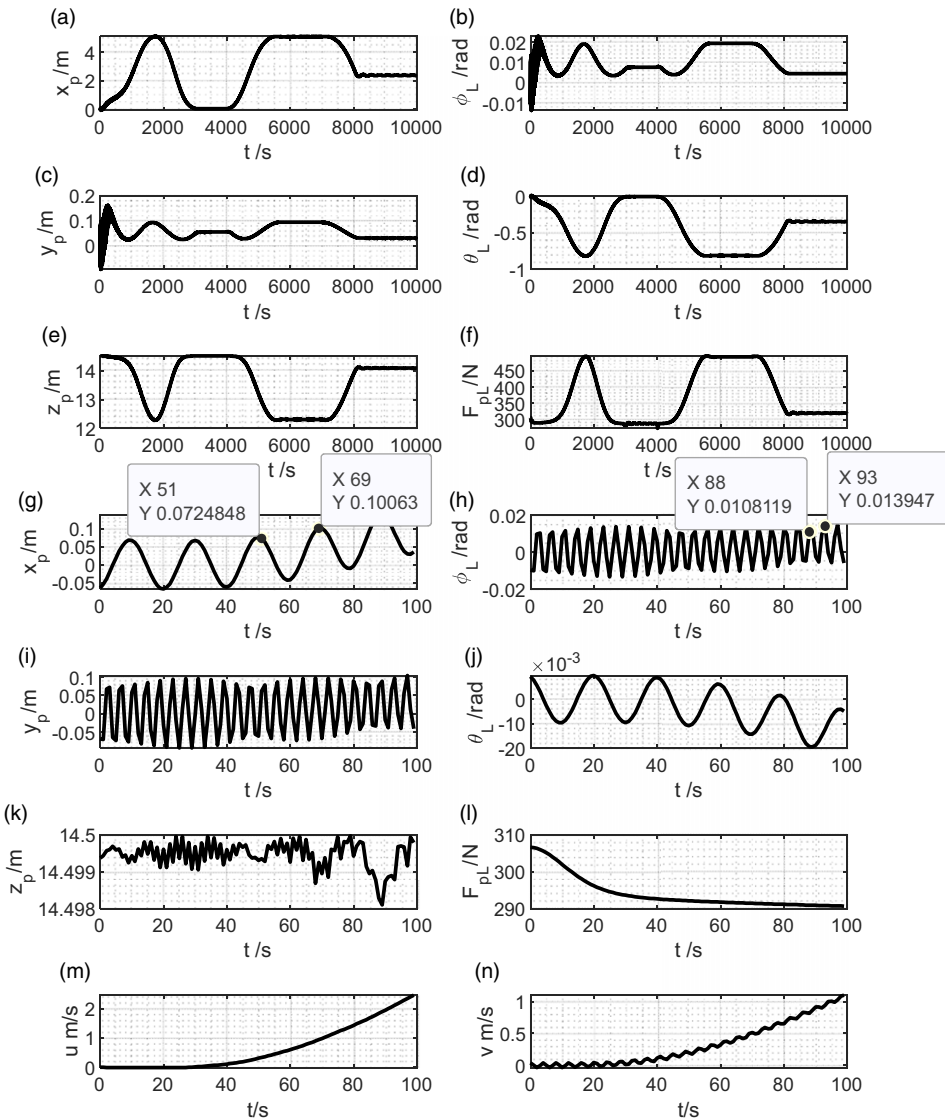


Figure 6. Vertical forces and acceleration of the platform.





**Figure 7.** Position and attitude of the pod and the cable force.

volume  $V_{He,t}$  at the target altitude. This volume ratio gradually approaches the target one as the platform reaches the target altitude. Hence, the ideal target altitude can be obtained.

The limitation of this controller is based on the assumption that the atmospheric density and pressure at the target altitude are obtained from a standard atmosphere model, which may be inaccurately determined. Thus, future work could establish an experimental model of atmospheric density and pressure in relation to altitude in a certain experimental area to eliminate altitude errors when the commanded pressure difference is reached [17].

**4.0 Simulation of manoeuvring process dynamics**

The simulation is divided into three phases: open ascending, autonomous descending and autonomous ascending. The target altitude is designed as

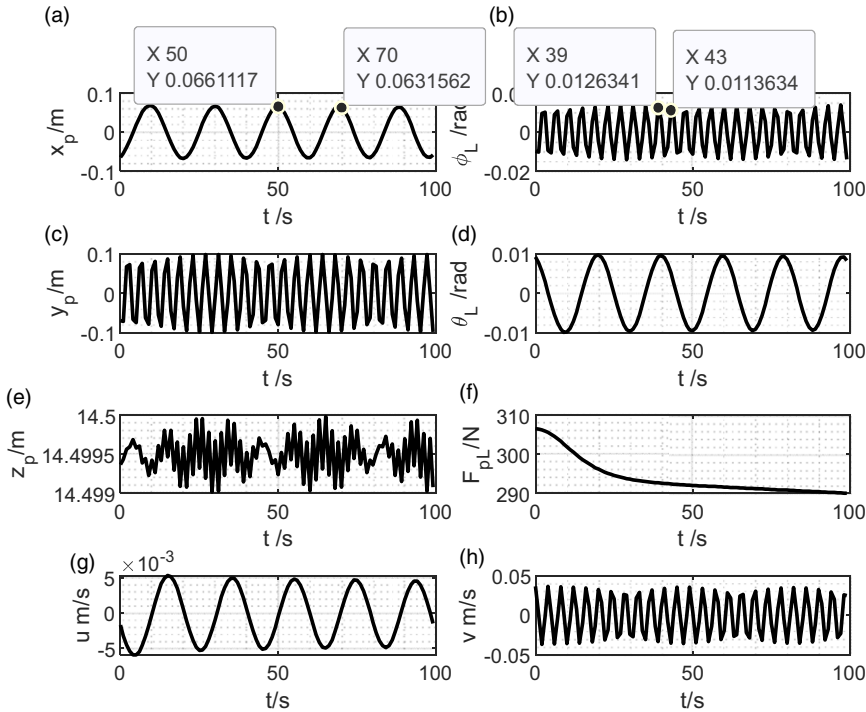


Figure 8. Position and attitude of the pod under a no-wind situation in a short period.

$$\begin{cases} h_t = 20km & (0 \leq t < 5000) \\ h_t = 10km & (5000 \leq t < 8000) \\ h_t = 15km & (8000 \leq t < 10000) \end{cases} \quad (46)$$

MATLAB is used to simulate the dynamics of the whole system. Firstly, the command ‘fsolve’ is applied to solve the dynamics of the whole system, as shown in Equation (33). Then, nine acceleration variables are obtained. The command ‘ode45’ is used to integrate the acceleration to obtain the position and attitude of the balloon. The acceleration of the pod is obtained from Equation (33), then ‘fsolve’ is employed to solve Equation (3) to acquire the angle of inclination of the pod.

In all flight simulations, the drag coefficient is 0.5 for the body and pod in all directions. The coefficient of virtual mass is 0.5. Heat transfer coefficient values and solar conditions can be found in Section 2.3.2. The numerical simulation results from this study are based on the selected model parameters. The simulation results for different parameters may vary in size, but the principles displayed in the simulation results will not change.

The simulation of the entire process of the platform is depicted in Figs 5–10. On the basis of the point mass dynamic equation, i.e. Equation (33), the thermodynamic parameters are adopted from Ref. (17). The variations in the state variable of the platform over time during the entire ascent and altitude change processes are shown in Fig. 5. Figure 5(a), (c) and (e) demonstrate the velocity change, and Fig. 5(b), (d) and (f) indicate the position change of the platform. The balloon is able to achieve flexible altitude changes, and its horizontal position drifts with the wind. Rather than using altitude as the control variable, this scheme adopts differential pressure difference; it can maintain a relatively stable tracking accuracy by avoiding the complexity of model calculation. Given that pressure difference is a slowly varying variable, the control response to differential pressure difference is delayed, and the overshoot

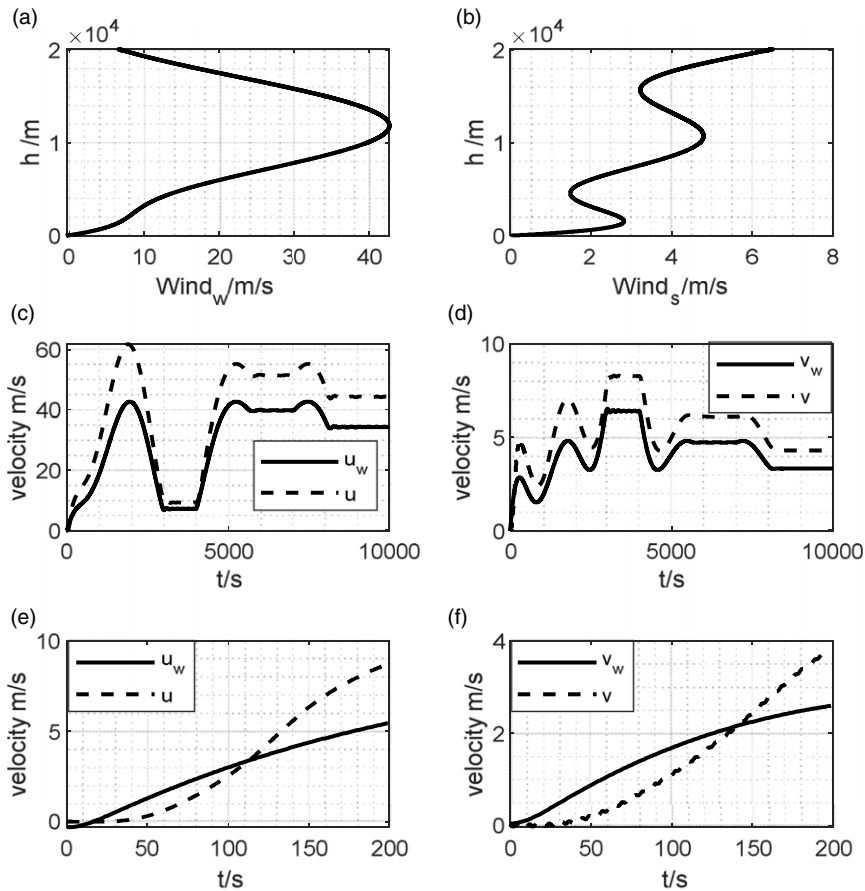


**Figure 9.** Horizontal motion of the platform in the wind field.

caused by the large inertia of the platform is inhibited, as shown in Fig. 5(f). The maximum vertical velocity reaches about 9m/s, as depicted in Fig. 5(e).

Figure 6 shows the vertical force and vertical acceleration of the platform. In the steady state, the platform lifts remain 6.5N, as illustrated in Fig. 6(c), and no vertical motion occurs, as shown in Fig. 6(d). The analysis of the dynamic equations indicates that the extra force is induced by the coupling of the nonlinear equation. Figure 6(d) shows that the maximum vertical acceleration is  $-0.28\text{m/s}^2$  at the initial condition and  $0.32\text{m/s}^2$  at the beginning of descending.

Figure 7 shows the position and attitude change of the pod and the force curve on the cable during the entire flight phases and in a short time. During the ascent, the forward angle of inclination  $\theta_L$  of the pod is close to  $-60^\circ$ , and the lateral angle of inclination  $\phi_L$  in the left and right directions does not change considerably. According to the definition of pod attitude angle, the forward direction of the platform is affected by the horizontal east–west wind, as shown in Fig. 8(b), resulting in the high forward movement speed of the platform depicted in Fig. 5(a), the forward position of the pod shown in Fig. 7(a) and the attitude angle fluctuations presented in Fig. 7(b). From Fig. 7(f), the maximum cable force does not exceed 500 N, which can be used for the designed lifting cable. Figure 7(h)–(k) indicate evidence for the pendulum motion of the pod. The oscillation period of the forward position and the forward angle of inclination is about 20s, as shown in Fig. 7(g) and (j). The oscillation period of the lateral position and the lateral angle of inclination is about 5s, as demonstrated in Fig. 7(h) and (i). The vertical position of the pod is oscillating with mixed frequencies, as shown in Fig. 7(k). The amplitude

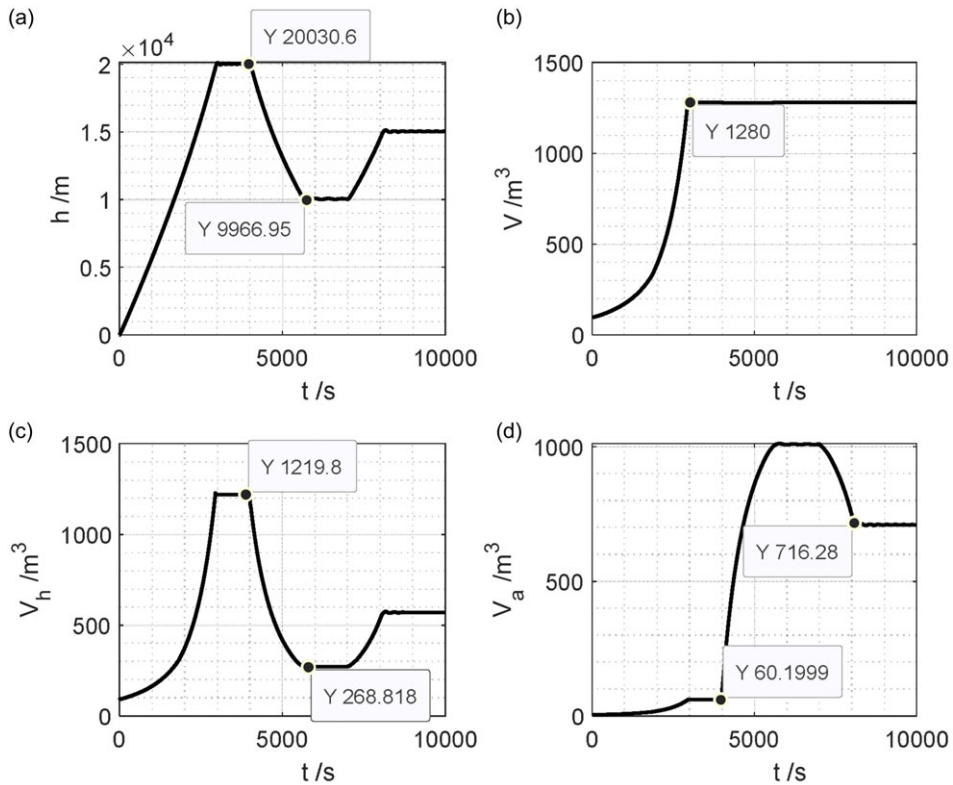


Figure 10. Volume variation in different phases.

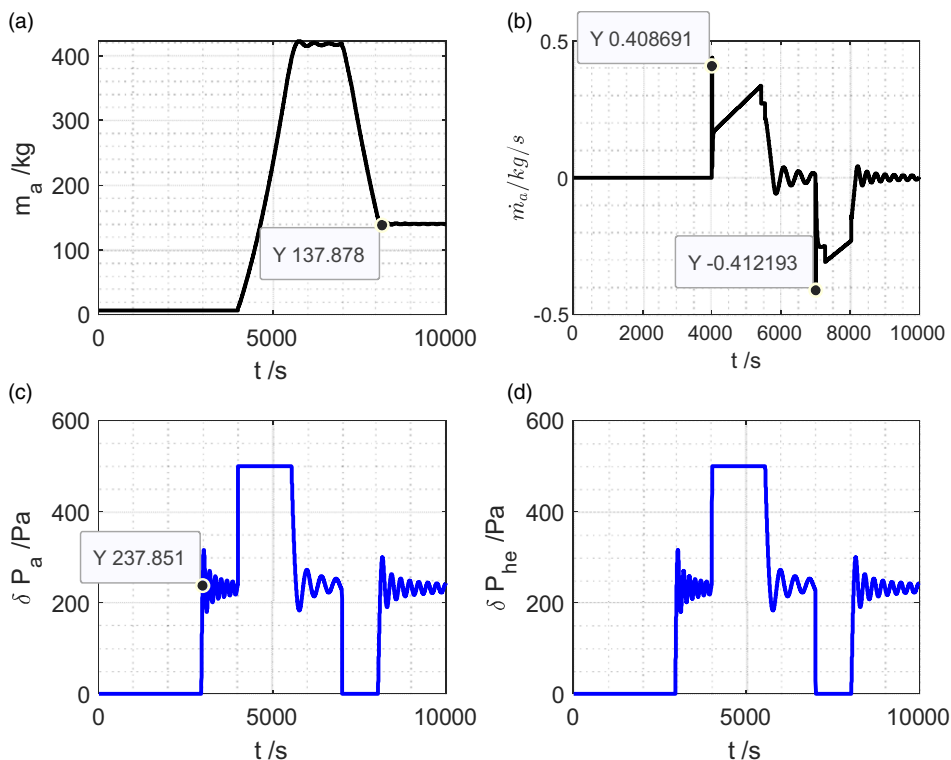
of pod oscillation motion is about 0.1 m, as illustrated in Fig. 7(g), (i) and (k), or has an attitude change of 0.01 rad, as shown in Fig. 7(h) and (j). No obvious oscillation in cable force occurs, as displayed in Fig. 7(l).

Figure 8 gives the position and attitude of the pod under a no-wind situation in a short period. The pendulum motion characteristic of the pod in Fig. 8(a)–(e) does not change compared with the wind situation, as shown in Fig. 7(g)–(k), whilst the balloon oscillates with the same frequency and a smaller amplitude of pendulum motion of the pod, as depicted in Fig. 8(g) and (h). The pod motion under the no-wind situation comprises that in the average-wind situation in Fig. 7, possibly indicating that the pendulum is moving with the platform motion in wind, as shown in Fig. 7(g)–(j).

Figure 9(a) and (b) show the wind field conditions at different heights of the platform, where Wind<sub>s</sub> is the wind from the south to the north, and Wind<sub>w</sub> is the wind from the west to the east. Figure 9(c) and (d) present the wind speed changes of the platform at different time phases. A comparison of body and wind velocities is shown in Fig. 9(c) and (d) for the whole process and in Fig. 9(e) and (f) for a short period. The platform passively drifts with the wind in the horizontal direction; however, their velocities differ, and an inertial overshoot of the body velocity over the wind velocity is observed.

The internal state of the high-altitude balloon is shown in Figs 10 and 11. The altitude reached is depicted in Fig. 10(a). The position error is about 30m higher than the set value because the stable pressure difference is about 240Pa at a balance altitude, as shown in Fig. 11(c), which is about 40Pa higher than the designed 200Pa. This error also results from the coupling effect of six nonlinear equations, given that the vertical motion is coupled with other motion.

The temperature differences in the whole process derived from thermodynamic models are shown in Fig. 12. The temperature of the ballonnet is related to the altitude variation and the charging or discharging of the ballonnet. Overheating of the helium balloon in natural expansion process during ascending time



**Figure 11.** Pressure difference in different phases.

occurs at about 2K, as exhibited in Fig. 12(b). An abrupt increase in ballonnet temperature occurs at the beginning of ballonnet charging, as demonstrated in Fig. 12(c) and (d). The change in temperature is closely related to the set parameters in Section 2.3.2.

These simulations validate the effectiveness of altitude control. The thermodynamic characteristic of the buoyancy body determines the buoyancy generated. The altitude holding error comes from the coupling of dynamics. The maximum pull force and maximum pod attitude angles during the ascending and descending processes provide basic knowledge for the structural design and load installation of pods.

## 5.0 Conclusion

This paper presents a modelling method and the theoretical analysis results of a high-altitude balloon with a slung pod as a combined system. Altitude adjustment of the high-altitude balloon is carried out with differential pressure difference as the control variable. The pressure difference change threshold is constrained by the blower flow rate. The controller can keep constant pressure difference at an arbitrary station-keeping altitude. The status and force of the balloon, pod and cable during the entire flight plan are simulated. The theoretical result of the maximum pull force of the cable is 500N. The forward inclination angle  $\theta_L$  of the pod reaches  $-60^\circ$ .

The mechanism analysis method presented in this paper can obtain a clear physical model, but numerous model variables need to be determined to generate a feasible solution in a high-altitude envelope. Thus, the results in this paper do not consider the dynamics of the cable and ignore the movement of the platform attitude. Structural dynamic software is suggested to be used for further numerical analysis to describe the dynamics of the motion process of the platform pod system thoroughly.

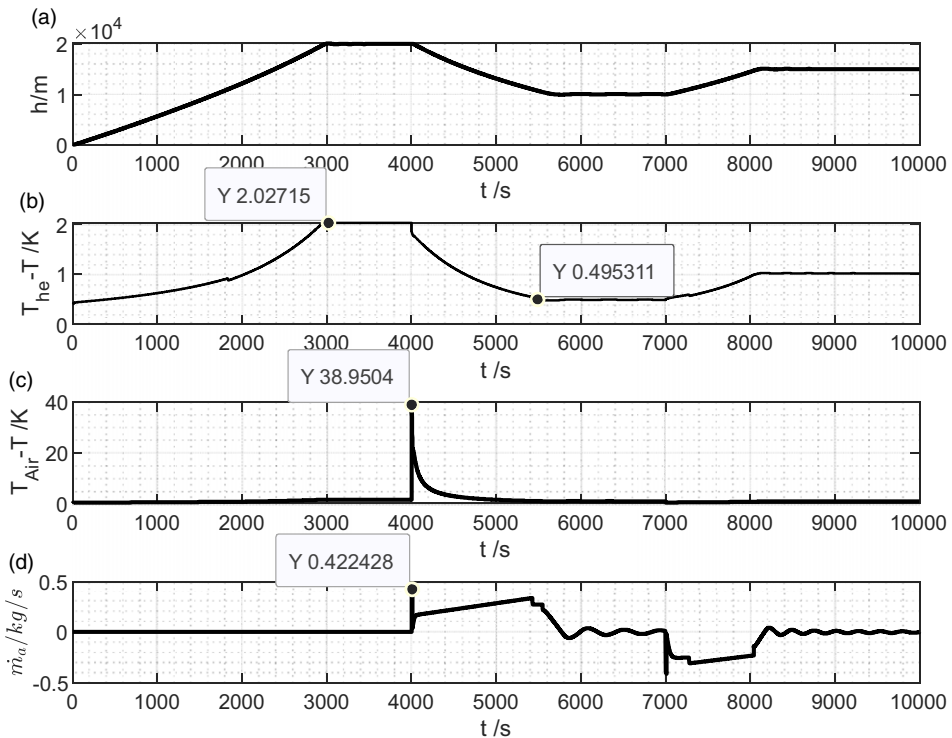


Figure 12. Temperature difference in various phases.

**Acknowledgement.** This research was funded by the National Natural Science Foundation of China (No. 52175103).

## References

- [1] d' Oliveira F.A., Francisco C.L. and Tessaleno, C.D. High-altitude platforms present situation and technology trends, *J. Aerospace Technol. Manag.*, 2016, **8**, (3), pp 249–262.
- [2] Andurkar A.G. and PrachiZodpe. A review paper on project “LOONS”, *Int. J. Adv. Res. Comput. Commun. Eng.*, 2016, **5**, (3), pp 132–138.
- [3] Oktay T. and Sultan C. Modeling and control of a helicopter slung-load system, *Aerospace Sci. Technol.*, 2013, **29**, pp 206–222
- [4] Pankine A., Li Z.Q. and Parsons D. Stratospheric satellites for earth observations, American Meteorological Society, August 2009, DOI: [10.1175/2009BAMS2624.1](https://doi.org/10.1175/2009BAMS2624.1)
- [5] Zaugg E.C., Margulis A., et al. SAR imaging from stratospheric balloons: first results, 2019 IEEE Radar Conference, DOI: [10.1109/RADAR.2019.8835692](https://doi.org/10.1109/RADAR.2019.8835692)
- [6] Sadr S., Moosavian A.A. and Zarafshan P. Dynamics modeling and control of a quadrotor with swing load, *J. Rob.*, 2014, Article ID 265897, 12 pp.
- [7] Hoh R.H., Heffley R.K. and Mitchell D.G. Development of Handling Qualities Criteria for Rotorcraft with Externally Slung Loads, NASA/CR-2006-213488, U.S. Army RDECOM No. AFDD/TR-06-003.
- [8] Stuckey R.A. Mathematical modelling of helicopter slung-load systems: DSTO-TR-1257 [R]. US, 2001.
- [9] Pal R.S. Modelling of helicopter underslung dynamics using Kane's method, *IFAC Papers On Line*, 2020, **53**, (1), pp 536–542.
- [10] Weber J.M. and Greif R.K. A Lagrange-D'Alembert formulation of the equations of motion of a helicopter carrying an externally suspended load, NASA Technical Memorandum 85864, 1985
- [11] Ardema M.D. Vehicle Concepts and Technology Requirements for Buoyant Heavy-Lift Systems, NASA Technical Paper, 1921, pp 1–19
- [12] Abdallah F.B., Hima S., Azouz N., Beji L. and Abichou A. Modeling and control of an airship-mounted crane for freight transportation, *IFAC Papers Line*, 2018, **51**, (9), pp 452–457.
- [13] Abdallah F.B., Azouz N., Beji L. and Abichou A. Modeling of a heavy-lift airship carrying a payload by a cable-driven parallel manipulator, *Int. J. Adv. Rob. Syst.*, 2019, **16**, (4), pp 1–17.

- [14] Bugga R., Jones J.P. and Pauken M. Extended-range variable altitude balloons for venus atmospheric missions, *Acta Astronautica*, 2022, **197**, pp 69–80.
- [15] Vandermeulen I., Guay M. and Mclellan P.J. Formation control of high-altitude balloons by distributed extremum seeking control, American Control Conference, IEEE, 2016, Boston, pp 2524–2529.
- [16] Borges R.A., Battistini S., Cappelletti C. and Honda Y.M. Altitude control of a remote-sensing balloon platform, *Aerospace Sci. Technol.*, 2021, **110**, p 106500.
- [17] Saleh, S. and He, W.L. Ascending performance analysis for high altitude zero pressure balloon, *Adv. Space Res.*, 2017, **59**, pp 2158–2172.
- [18] Öznur, K.M. and Alaïttin, H. Modeling of stratospheric balloon using transport phenomena and gas compress–release system, *J. Thermophys. Heat Transfer*, 2014, **28**, (3), pp 534–541.
- [19] Shi H., Song B.Y., and Yao Q.P. Thermal performance of stratospheric airships during ascent and descent, *J. Thermophys. Heat Transfer*, 2009, **23**, (4), pp 816–821.
- [20] Carlson L.A. and Horn W.J. New thermal and trajectory model for high-altitude balloons, *AIAA J. Aircraft*, 1983, **20**, (6), pp 500–507.
- [21] Schallenkamp R.S., Siewert A.D. and Lachenmeier T.T. Parametric analysis Of Overpressure Zero Pressure (OZP) balloons using the SINBAD computer model, 32nd Aerospace Sciences Meeting & Exhibit, January 10-13, 1994/ Reno, NV AIAA 94-0515.